

Article

A Back-Drivable Rotational Force Actuator for Adaptive Grasping

Xiaofeng Wu ^{1,2}, Hongliang Hua ^{1,3,*}, Che Zhao ^{1,*}, Naiyu Shi ¹ and Zhiwei Wu ^{4,*}

¹ School of Aeronautics and Mechanical Engineering, Changzhou Institute of Technology, Changzhou 213032, China

² Shandong Lingong Construction Machinery Co., Ltd., Linyi 276023, China

³ School of Mechanical Engineering, Nanjing University of Science and Technology, Nanjing 210094, China

⁴ College of Art and Communication, China Jiliang University, Hangzhou 310018, China

* Correspondence: huah123@126.com (H.H.); zhaoche@czu.cn (C.Z.); 20a1302033@cjlu.edu.cn (Z.W.)

Abstract: In this paper, a back-drivable and miniature rotary series elastic actuator (RSEA) is proposed for robotic adaptive grasping. A compact arc grooves design has been proposed to effectively reduce the dimension of the RSEA system. The elastic elements could be reliably embedded in the arc grooves without any additional installation structures. The whole RSEA system is characterized as compact, miniature, and modular. The actuating force is controlled via a PI controller by tracking the deformation trajectory of the elastic elements. An underactuated finger mechanism has been adopted to investigate the effectiveness of the RSEA in robotic adaptive grasping. Results reveal that the underactuated finger mechanism could achieve adaptive grasping via the RSEA in a back-drive approach without the requirement of a fingertip force sensor. The RSEA could also exhibit an actuating compliance and a self-sensing characteristic. The actuating compliance characteristic helps in guaranteeing the safety of human–robot interaction. The RSEA could estimate the external disturbance due to its self-sensing characteristic, which has the potential to replace the fingertip force sensor in grasping force perception applications.

Keywords: robotic grasping; actuator; series elastic actuating; adaptive grasping



Citation: Wu, X.; Hua, H.; Zhao, C.; Shi, N.; Wu, Z. A Back-Drivable Rotational Force Actuator for Adaptive Grasping. *Actuators* **2023**, *12*, 267. <https://doi.org/10.3390/act12070267>

Academic Editor: Rocco Antonio Romeo

Received: 20 May 2023

Revised: 18 June 2023

Accepted: 21 June 2023

Published: 29 June 2023



Copyright: © 2023 by the authors. Licensee MDPI, Basel, Switzerland. This article is an open access article distributed under the terms and conditions of the Creative Commons Attribution (CC BY) license (<https://creativecommons.org/licenses/by/4.0/>).

1. Introduction

Robotic gripper is a fundamental component of the robot which helps it achieve grasping operations and it has a broad application background in agricultural picking [1–3], food packing [4–7] and minimally invasive surgery [8–10]. Safety, adaptability, easy actuation and control are the essential requirements for the robotic gripper [11–14]. One of the important aspects to fulfil these aforementioned requirements is grasping force control. Through grasping force control, the robotic gripper could grasp the object in an adaptive, stable and non-destructive manner [15–17].

At present, there exists three main approaches to achieve grasping force control: motor torque control [18], pneumatic actuator [19,20], and series elastic actuating technology [16,17]. Combined with the fingertip force sensor, the motor torque control method could directly achieve grasping force control [21–23]. However, this method could increase the difficulty of wire routing. Furthermore, large number of the sensor could significantly increase the control complexity of the gripper. Pneumatic actuation has been proven to be effective in force control of robotic grippers [20]. The grasping force could be controlled by calibrating its relation with respect to the actuating pressure. However, due to the nonlinear hysteresis characteristic of the pneumatic actuator, the relation between the grasping force and actuating pressure could be time-varying, thereby making it difficult to identify [24,25]. From the perspective of force sensing and actuating, the series elastic actuating approach is more suitable for robotic grasping. Compared to the pneumatic actuator, the stiffness of the SEA is relatively constant, which is advantageous for control modeling. Series elastic actuator (SEA) generally refers to introducing an elastic element between the rigid actuator and final output mechanism. On

one hand, the SEA have an inherent actuating compliance due to the existence of the elastic element in the transmission link. Therefore, the grasping safety could be easily guaranteed [15]. On the other hand, the external force which exists in the actuating link could be precepted by the SEA without the requirement of the fingertip sensor.

Taking into consideration the simplicity, compactness, and safety requirement of the robotic gripper, we present a rotary series elastic actuator (RSEA) which could actuate the robotic gripper in a back-drive approach. Currently, the series elastic actuator is mainly applied to legged robots [26,27], cooperative robot joint [28,29] and knee joint assistive systems [30–32]. In these applications, the series elastic actuator research focuses on the instantaneous high power output ability. According to the existing literature, there are few reports on the studies about the series elastic actuator in robotic gripper or hand. For the robotic gripper or hand applications, the series elastic actuator research will focus on the aspects of actuating compliance, external force sensing and control performance [17]. In our previous work [17], a linear series elastic actuator (LSEA) has been developed and applied to the anthropomorphic and underactuated grasping system [16]. Results reveal that the SEA-actuated grasping system could significantly reduce the control overshoot and obtain an ideal grasping effect. Inspired by our previous work, we are motivated to develop a rotary-type SEA to provide a novel view of developing rotary series elastic actuator for the robotic community. In the present study, the proposed RSEA is characterized as compact, and modular, which could effectively reduce the integrating difficulty of the robotic grasping system. The grasping adaptability and safety could be achieved via the RSEA in a feedforward way without the requirement of a fingertip force sensor. This could further reduce the mechanical and control complexity of the robotic grasping system.

The rest of this paper is organized as follows: In Section 2, the design considerations and force control strategy are introduced. Section 3 presents the experimental results and its discussion. Conclusions are presented in Section 4.

2. Design and Control Methods

2.1. Mechanical Design

The proposed miniature compact RSEA is displayed in Figure 1. The RSEA is mainly composed of micro servo motor, driving flange, output flange, encoder, and linear springs. The driving flange is mounted on the output shaft of the micro servo motor to actuate the output flange. Two linear springs are designed between the driving flange and output flange to transmit the rotation motion in an elastic manner. The two springs are embedded in the arc grooves of the driving flange and output flange, as shown in Figure 2a. The driving flange and the output flange are assembled by a thin-walled bearing to ensure that they are concentric. As the driving flange and output flange rotate relatively, the springs will be compressed and produce a resilience. In this way, driving torque of the driving flange will be transmitted to the output flange elastically. The driving torque is a function of the relative rotation angle between the driving flange and output flange. The relative rotation angle can be measured via a rotary encoder embedded on the surface of the output flange. An output swing arm and wire wheel are designed on the output flange for the convenience of subsequent experimental research.

As depicted in Figure 2a,b, two arc grooves are symmetrically designed on the driving and output flanges to achieve bidirectional actuating. Each arc groove contains a limit surface pair, those are a&b, c&d, A&B, and C&D, respectively. Limit surface pairs a&b and c&d belong to the driving flange, while A&B and C&D belong to the output flange. Under the action of the spring's resilience, limit surface A and a, B and b, C and c, and D and d will align automatically. As an external load F_0 is applied to the output flange, a relative angular offset θ_c will appear between the driving flange and output flange. When the output flange is actuated to rotate clockwise with respect to the input flange, two springs will be compressed by limiting surfaces a&B and c&D. In the same way, two springs will be compressed by limiting surfaces A&b and C&d as the output flange rotates counter clockwise. Due to the arc grooves, the axial size from driving flange to the output flange

of the RSEA can be effectively reduced, which is 11.5 mm in the presented design. As shown in Figure 2a, the springs could be embedded in the arc grooves reliably without any additional installation structures. It should be noted that the groove needs to be filled with an appropriate amount of lubricating grease before the assembly. In this way, the effect of the friction between the springs and the groove on the final force control could be significantly reduced. Thus, the whole RSEA system could achieve simplicity and compactness which will be sufficient for the applications in robotics, such as robotic hand. Finally, the overall dimension, weight and maximum driving torque of the RSEA are $42.5 \text{ mm} \times 34 \text{ mm} \times 62 \text{ mm}$, 85 g and 2 Nm, respectively. It is worth noting that for the proposed RSEA configuration, its dimension could be further reduced. However, this could lead to the decrement of the peak torque. The RSEA prototype design in this study is a balance between the dimension and actuating ability.

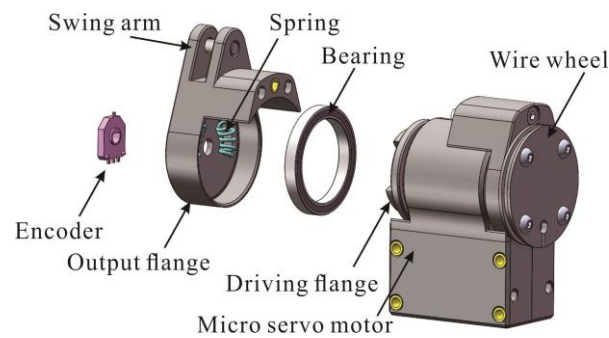


Figure 1. 3D CAD illustration of the RSEA system.

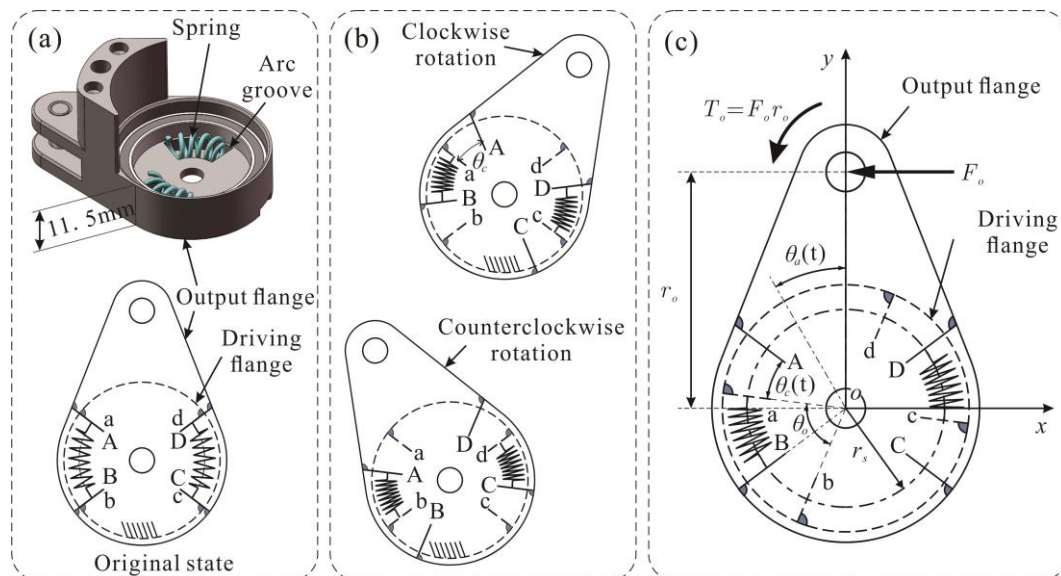


Figure 2. Actuating principle of the RSEA. (a) Arc grooves design. (b) Principle of torque transfer. (c) Torque and spring deformation analysis.

According to the relative angular offset θ_c , the output torque T_o of the output flange could be given as,

$$T_o = 2kr_s(l_{s0} - r_s\theta_o + r_s\theta_c) \quad (1)$$

where, k , r_s and l_{s0} denote the spring stiffness, radius of the spring centerline and spring original length, respectively. θ_o denotes the angle of the arc grooves of the driving flange and output flange. It should be noted that spring stiffness k is unknown for its bending deformation. In addition, the spring deformation characteristic could be further affected by the friction between the springs and the groove. To address this problem, the groove

needs to be filled with an appropriate amount of lubricating grease before the assembly. In this way, the effect of the friction between the springs and the groove on the final force control could be significantly reduced, and the tangential force from the spring becomes a negligible item. In the present study, the tangential force is neglected. From Equation (1) it is found that the torque output characteristics of the RSEA could be modified by different spring stiffness k and original length l_{s0} . When RSEA move to its original state, $\theta_c = 0$, Equation (1) becomes,

$$T_{oi} = 2kr_s(l_{s0} - r_s\theta_o) \quad (2)$$

where, T_{oi} denotes the initial output torque of the RSEA under the action of spring pre-pressure. It indicates that $l_{s0} > r_s\theta_o$ should be fulfilled to guarantee a positive T_{oi} , otherwise the original state of the RSEA will be unstable. Generally, a larger l_{s0} and k could achieve a larger initial output torque T_{oi} .

2.2. Model Identification and Control

According to Equation (1), a target output torque T_o could be controlled by tracking θ_c . To obtain the relation between the output torque T_o and the relative rotation angle θ_c , a model identification experiment has been conducted, as shown in Figure 3. As output flange rotates clockwise and contact with the Y-type contact of the force gauge, its rotation will be limited by the Y-type contact and apply a horizontal force F_o to the force gauge, see Figure 3a. In this way, F_o could be measured by the force gauge directly. Then, the output torque T_o could be obtained as $T_o = F_o r_o$, as illustrated in Figure 2c. In experimental tests, the loading and unloading process has been repeated for three rounds to observe the hysteresis and the repeatability characteristics of the SEA system. The relative rotation angle θ_c between the driving flange and output flange is measured via the rotary encoder which is embedded on the surface of the output flange, as depicted in Figure 1.

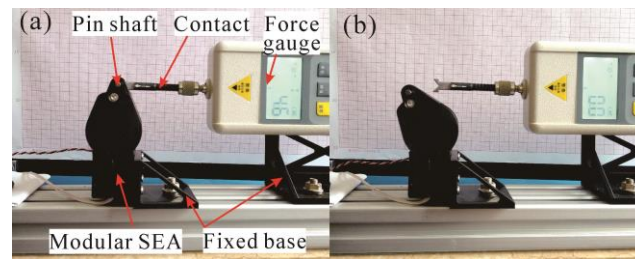


Figure 3. Experimental platform to measure the actuating force of the SEA system. (a) Unloading state. (b) Loading state.

The polynomial model has been adopted to design the relation between F_o and θ_c . Two error variables, $\|E_F\|_2$ and $\|E_\theta\|_2$, have been utilized to evaluate the fitting accuracy of the relation between F_o and θ_c . Here, $E_F = \tilde{F}_o - F_o$ and $E_\theta = \tilde{\theta}_c - \theta_c$. Generally, the smaller $\|E_F\|_2$ and $\|E_\theta\|_2$ denote a better fitting accuracy of the F_o and θ_c , respectively. $\|E_F\|_2$ and $\|E_\theta\|_2$, with respect to different model order n ranges from 1 to 10, have been computed and plotted in Figure 4a. From Figure 4a, it could be observed that the decrement in $\|E_F\|_2$ and $\|E_\theta\|_2$ is relatively small as the model order n increases. Taking into consideration the fitting accuracy and computing cost, first and second-order approximate models have been adopted for F_o and θ_c , respectively, as

$$\tilde{F}_o = 0.1554\theta_c - 0.4165 \quad (3)$$

$$\tilde{\theta}_c = -0.3374F_o^2 + 7.5118F_o + 3.5238 \quad (4)$$

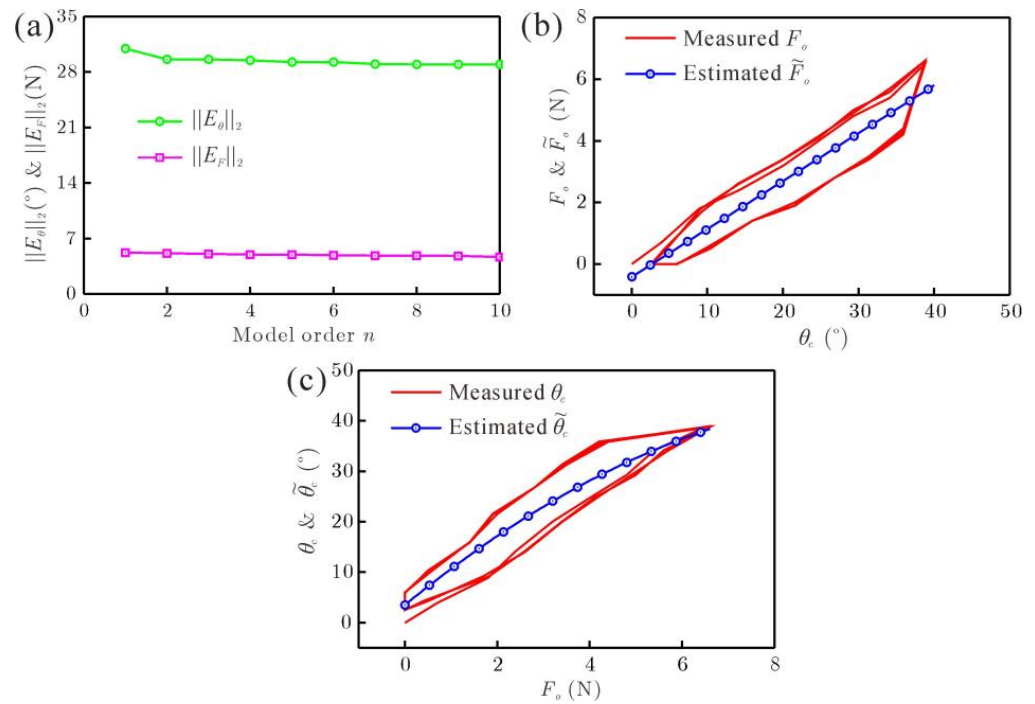


Figure 4. Model identification of F_o and θ_c . (a) Fitting error $\|E_F\|_2$ and $\|E_\theta\|_2$ with respect to different model order n . (b) Comparison between \tilde{F}_o and F_o . (c) Comparison between $\tilde{\theta}_c$ and θ_c .

The identified \tilde{F}_o and $\tilde{\theta}_c$ are compared to the experimental response in Figure 4b,c, respectively. From Figure 4b,c it could be observed that the experimental relation between F_o and θ_c exhibits a hysteresis characteristic. Therefore, Equations (3) and (4) will have certain approximate error over the whole range. The actuating force F_o could be precepted using Equation (3) and then measure θ_c . Equation (4) could be utilized to generate the tracking target $\tilde{\theta}_c$ by a given target actuating force F_o .

In the proposed RSEA, a micro servo motor is utilized to actuate the driving flange. A PI controller is adopted to eliminate the tracking error of θ_c as,

$$\begin{cases} \theta_a = K_p e + K_i e_{sum} \\ e = \tilde{\theta}_c - \theta_{c,j} \\ e_{sum} = \sum_{j=1}^n e_j \end{cases} \quad (5)$$

where, θ_a denotes the actuating angle of the driving flange. e denotes the tracking error between the target springs deformation trajectory $\tilde{\theta}_c$ and real-time springs deformation $\theta_{c,j}$. Subscript j represents the time series. K_p and K_i are proportional and integral constants of the PI controller. In the present study, an optimal $K_p = 0.07$ and $K_i = 0.005$ have been adopted via the trial-and-error method. During the trial-and-error process, we set $K_i = 0$ at first and increase the K_p gradually to accelerate the response of the actuating force to obtain an ideal rising characteristic. And then the K_i was gradually increased to reduce the steady state error. It is worth noting that a PID controller could also achieve an equivalent control effect as the PI controller. In control experiments, we found that the rotation speed of the RSEA is relatively lower, and the D term of the PID controller could not significantly improve the control performance of the RSEA but increase the difficulty of parameters tuning. The I term of Equation (5) is helpful to eliminate the tracking error to a certain extent. Therefore, the PI controller is more appropriate for the RSEA when compared to the others.

3. Experimental Results and Discussion

3.1. Step Response

A step response experiment has been conducted to evaluate the step response characteristic of the RSEA based on the experimental platform, as shown in Figure 3. In this experiment, Equation (4) has been adopted to generate the tracking target $\hat{\theta}_c$ by substituting F_o with a certain target actuating force t_F , and Equation (3) has been utilized to estimate the actuating force F_o by measuring the spring deformation θ_c . Since the RSEA prototype is 3D-printed using polylactic acid (PLA) material, a larger actuating torque could lead to the structure damage. Therefore, the step force control experiment is performed within a lower level. In control test, we found that the actuating force has a dead zone of about ± 1.2 N. In this range, the actuating force control is unstable. Taking into consideration the above factors, the target actuating force is set as 2 N to 7 N. The step response of the target actuating force t_F range from 2 N to 7 N with an increment of 1 N have been investigated experimentally, and the obtained step response are displayed in Figure 5. From the response, it could be observed that the settling time of the force control is about 0.35 s for the different target actuating forces. The maximum steady-state error is about 0.15 N, and no overshoot occurs. To investigate the control accuracy of the RSEA system, the control error and estimation error is defined as,

$$\begin{aligned} e_{\text{con}} &= \frac{|F_o - t_F|}{t_F} \times 100\% \\ e_{\text{est}} &= \frac{|\tilde{F}_o - F_o|}{t_F} \times 100\% \end{aligned} \quad (6)$$

where, F_o denotes the measured actuating force by force gauge. Taking into consideration the force control repeatability, the step response experiment for each t_F have been performed for three times. The control error with respect to different t_F is displayed in Table 1. It could be observed that in producing smaller actuating force, the control error is relatively larger. For a 2 N actuating force, the control error is about 20%. As the actuating force increases, the control accuracy will be improved. However, for some points, such as 5 N, the control error is still large. This phenomenon could be attributed to that the deformation of the linear spring exhibiting an obvious hysteresis characteristic, as depicted in Figure 4b. As a result, the model identification will inevitably yield an obvious modeling error and lead to the control error. In future work, the stiffness of the linear spring should be carefully evaluated.

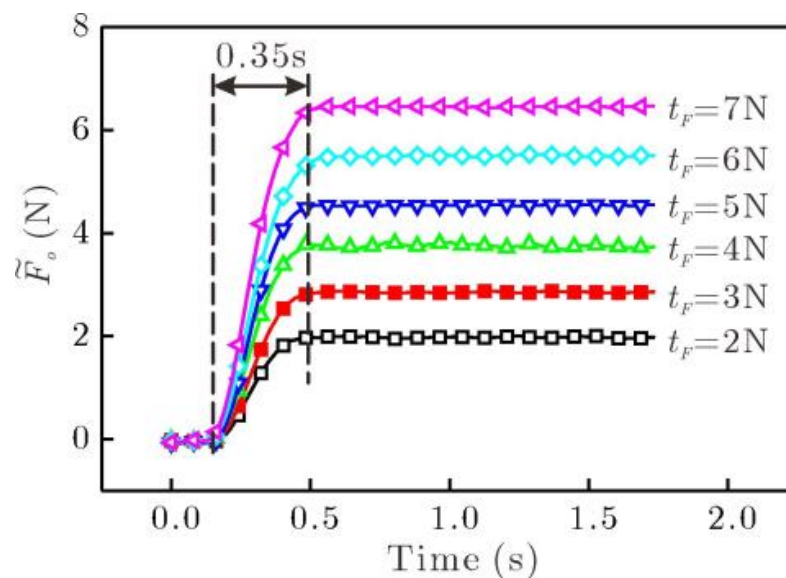


Figure 5. Control responses of the RSEA with respect to different t_F actuating force.

Table 1. Control accuracy analysis.

t_F (N)	Measured F_o (N)	e_{con} (%)	Estimated \tilde{F}_o (N)	e_{con} (%)
2	2.4	20	2.0	−16.7
3	3.0	3.3	2.8	−6.7
4	3.9	−2.5	3.8	−2.6
5	4.5	−10	4.6	2.2
6	5.6	−6.7	5.5	−1.8
7	7.1	1.4	6.8	−4.2

For robotic grasping applications, adaptive interaction with the uncertain environment is an essential requirement. To further investigate the response characteristic of the RSEA in interacting with the external environment with uncertain stiffness, the rigid Y-type contact of the force gauge has been replaced by an O-type rubber ring with hyper elasticity and nonlinear deformation characteristics, as shown in Figure 6a. Since the O-type rubber ring is more suitable to bear a tension force, therefore, the target actuating force in this experiment is set as -2 N to -6 N, with an amplitude increment of -1 N. In this way, the RSEA will apply a force to the O-type rubber ring horizontally to the left. It should be noted that the main purpose of this experiment is to investigate the response characteristic of the RSEA in interacting with the external environment with uncertain stiffness, rather than to investigate the force control accuracy. The direction of the actuating force is time-varying in this experiment. Some motion sequences of the interaction between RSEA and O-type rubber ring is given in Figure 6a–f. The response of the actuating force is displayed in Figure 6g. From the response, it could be observed that the actuating force of the RSEA will experience three phases to achieve the final control steady state. In phases 1 and 3, the actuating force response rapidly. While in phase 2, the RSEA will experience a short-term steady state. This phenomenon is due to the deformation hysteresis characteristic of the O-type rubber ring. After the end of phase 2, the deformation hysteresis disappears and the RSEA will continue to respond rapidly and achieve the final steady state. From Figure 6g, it could be observed that the settling time of each t_F is about 2.27 s, 1.21 s, 1.59 s, 1.74 s and 1.70 s, respectively, which is significantly longer than that of the rigid objects. From the response of the actuating force, it could be observed that the RSEA could achieve final steady state at different actuating force level. Above all, the O-type rubber ring loading experiment could effectively simulate the response characteristic of the RSEA in interacting with the external environment of uncertain stiffness. And the effectiveness of the force controller could also be investigated.

3.2. Adaptive Grasping Experiment

A tendon-driven underactuated finger mechanism has been adopted as the grasping mechanism to investigate the effectiveness of the miniature RSEA in adaptive grasping. The finger mechanism is mainly composed of proximal phalange, middle phalange, distal phalange, tension tape and tendon. The experimental platform is depicted in Figure 7. Generally, a larger pre-tension force of the tension tape could increase the stiffness of the finger mechanism. However, it requires a larger actuating force for the finger mechanism to produce grasping motion and affect the peak value of the grasping force. Taking into account the above considerations, the pre-tension force of the tension tape of the present finger mechanism is designed as about 1.4 N by selecting an appropriate length of the tension tape. In experiment, the tendon is actuated by the wire wheel which is mounted on the RSEA output flange. As the wire wheel rotates counterclockwise, the tendon will be tensioned and will actuate the finger mechanism to produce bending motion, which could be utilized to achieve object grasping.

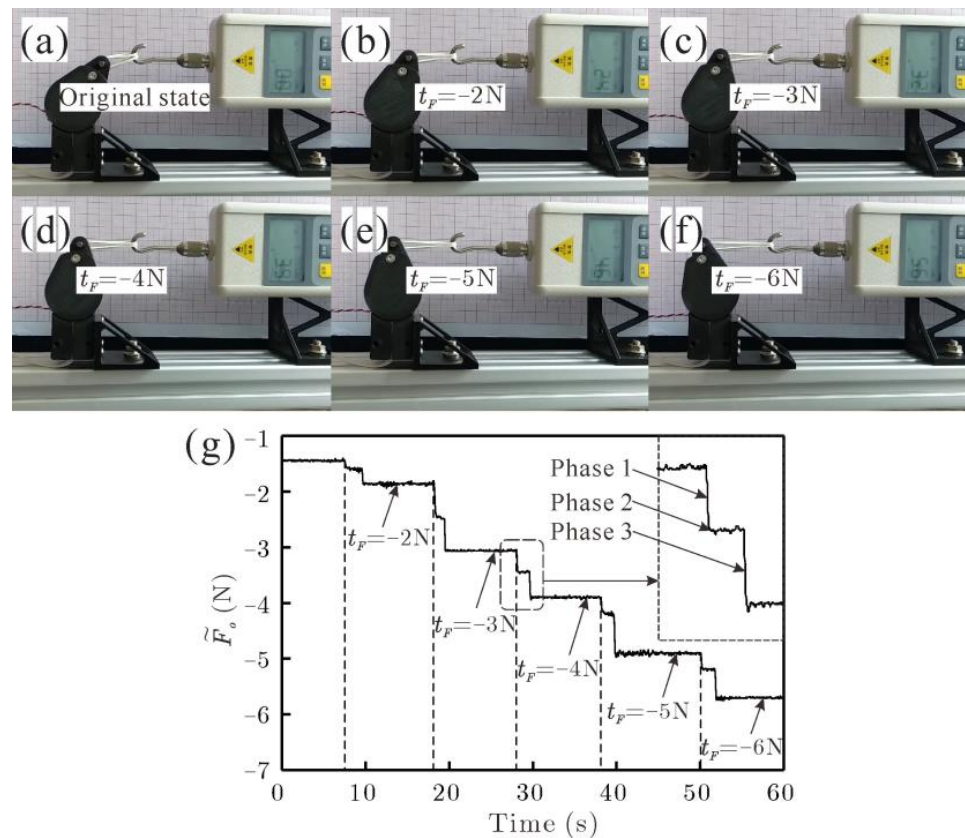


Figure 6. O-type rubber ring loading experiment. (a) Original state. (b–f) Steady state of the rubber ring under different t_F ranges from -2 N to -6 N . (g) Self-sensed response of the actuating force under different t_F ranges from -2 N to -6 N .

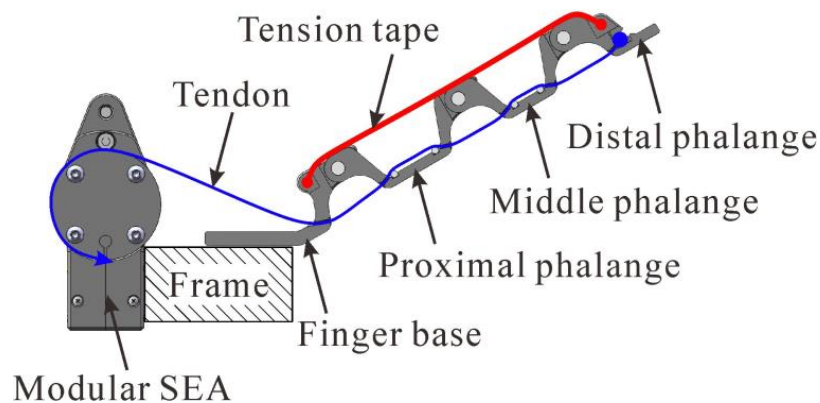


Figure 7. Experimental setup for underactuated figure mechanism actuation.

For the grasping experiment, an elastic ball with a diameter of 55 mm has been adopted as the grasping object. The corresponding grasping process is displayed in Figure 8 using some typical motion sequences of the finger mechanism. In Figure 8b, the whole finger structure rotates around the finger base. In Figure 8c, the motion of the proximal phalange is blocked after it comes into contact with the grasping object, and the remaining phalanges will continue to rotate around the proximal phalange as shown in Figure 8d. Subsequently, the middle and distal phalange will come into contact with the grasping object in the same way and achieve an equilibrium state under the action of the actuating force as shown in Figure 8f. In Figure 8g–l, the target actuating force is set as 0 and the object is released from the underactuated finger mechanism.

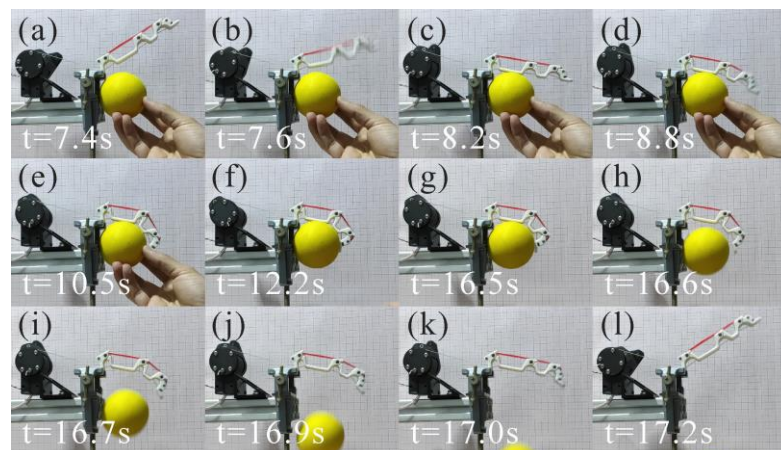


Figure 8. Adaptive grasping process of the underactuated finger mechanism. (a–f) Object grasping process. (g–l) Object releasing process.

Actuating force with different amplitudes, -5 N and -10 N, has been applied to the underactuated finger mechanism to evaluate its effect on grasping performance. The final grasping state of the different actuating force is compared in Figure 9a,b. The response of the self-sensed actuating force is compared in Figure 9c. From Figure 9a,b, it could be observed that for a 5 N actuating force, the proximal and middle phalanges will come into contact with the grasping object. Since the distal phalange requires a larger actuating force than that of the proximal and middle phalanges, therefore, the distal phalange have not come into contact with the grasping object under this circumstance. On the other hand, for a 10 N actuating force, all the three phalanges have come into contact with the grasping object and achieve a better adaptive grasping state as depicted in Figure 9b. From Figure 9c, it could be observed that the settling times of -5 N and -10 N actuating force are about 3.1 s and 1.2 s, respectively. It reveals that increase in the actuating force could accelerate the grasping process to some extent. This phenomenon could be attributed to the nonlinear bending motion characteristic of the underactuated finger mechanism. The smaller actuating force control is more sensitive to the nonlinear disturbance of the underactuated finger mechanism. The aforementioned grasping experiments reveal that the proposed RSEA is suitable for adaptive grasping applications. The grasping strength of the finger mechanism could be controlled via the RSEA in a back-drive approach without the requirement of a fingertip force sensors. This could significantly reduce the complexity of the finger mechanism. To further enhance the perception accuracy of the grasping force, a refined kinematic or dynamic model of the finger mechanism is essential to compensate for the influences of the grasping state; this requires further in-depth research efforts.

An interactive experiment between RSEA actuated finger mechanism and human finger has been conducted to investigate the adaptability and safety of the RSEA in the robot–human interaction applications. In this experiment, a -5 N actuating force is utilized to actuate the finger mechanism to move to a grasping state as shown in Figure 10a. The corresponding response of the actuating force of the RSEA, which is obtained because of its self-sensing ability, that is Equation (3), is displayed in Figure 10i, the green and transparent area. Then, a series of unstructured human disturbance (in Figure 10i, the red and transparent area) is applied to the finger mechanism which disturbs the force controller of the RSEA system. As depicted in Figure 10b–e, the finger mechanism is forced by the human finger to move to the original state passively. In this process, the RSEA exhibits a compliant actuating characteristic. For the human–robot interactive grasping applications, this characteristic is helpful to guarantee the safety of the human. In Figure 10f–h, the external disturbance disappears and the finger mechanism moves to the grasping state under the actuation of the RSEA. The corresponding response of the self-sensed actuating force of the RSEA is displayed in Figure 10i, the blue and transparent area. Experimental results further reveal that the external disturbance could be precepted via the RSEA in a

back-drive manner, which has the potential to replace the fingertip force sensor in grasping force perception applications.

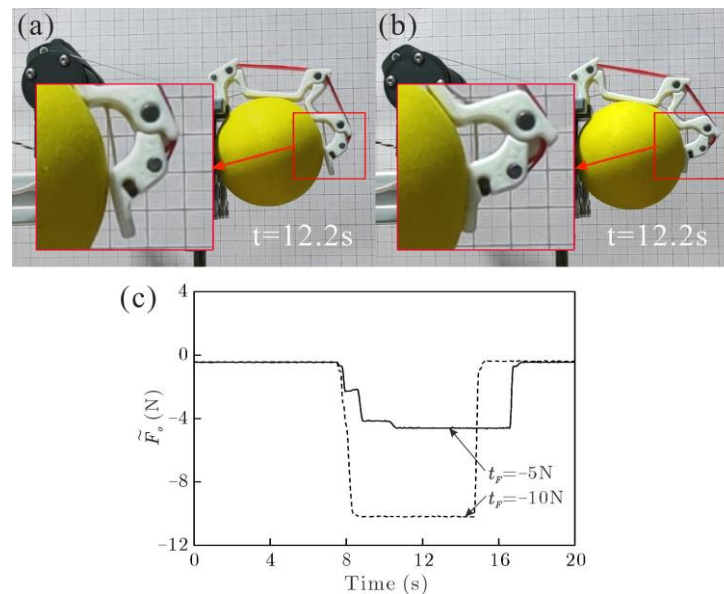


Figure 9. Object grasping state under different actuating force. (a) Actuating force = 5 N. (b) Actuating force = 10 N. (c) Self-sensed actuating force under different control target.

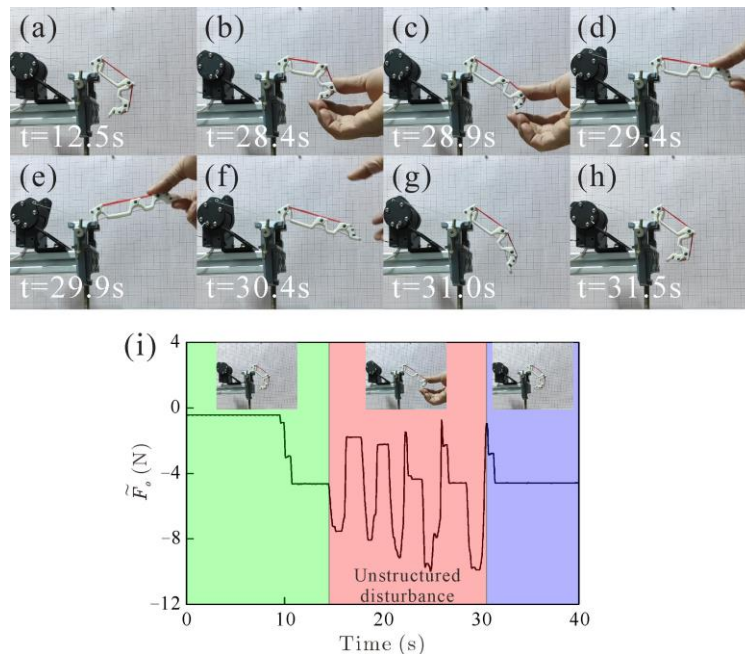


Figure 10. Interaction with a human hand. (a–h) Motion sequences of the interaction. (i) Actuating force response.

4. Conclusions

In this paper, a miniature compact RSEA is presented for robotic adaptive grasping applications. An arc grooves design is proposed to effectively reduce the dimension of the RSEA system. The springs could be embedded reliably in the arc grooves without any additional installation structures. In this way, the miniaturization and compactness of the whole RSEA system could be adequately ensured for the robotic grasping applications.

An underactuated finger mechanism has been adopted to validate the effectiveness of the RSEA in robotic adaptive grasping. The underactuated finger mechanism could achieve

adaptive grasping via the RSEA in a back-drive approach without the requirement of a fingertip force sensor. The grasping strength of the object could be controlled by different actuating forces. For a certain grasping object, a larger actuating force could reduce the settling time of the object grasping.

RSEA exhibits a compliant actuating characteristic. For the human–robot interactive grasping applications, this characteristic is helpful to guarantee the human safety. In addition, the external disturbance could be precepted via the RSEA because of its self-sensing ability, which has the potential to replace the fingertip force sensors. To further enhance the perception accuracy of the grasping force, a refined kinematic or dynamic model of the finger mechanism is essential to compensate for the influences of the grasping state; this requires further in-depth research efforts.

Author Contributions: Conceptualization, H.H.; Methodology, all authors.; Software, X.W.; Validation, N.S. and Z.W.; Investigation H.H.; Data curation, X.W.; Writing—original draft preparation, X.W.; writing—review and editing, H.H. and C.Z.; Funding acquisition, H.H. and C.Z. All authors have read and agreed to the published version of the manuscript.

Funding: This research was funded by the China Postdoctoral Science Foundation, under Grant 2022M721613, the National Natural Science Foundation of China under Grant 52105295, 32201673, the Natural Science Foundation of Jiangsu Province under Grant BK20210082 and the Natural Science of Foundation of the Jiangsu Higher Education Institutions of China under Grant 20KJA460006, 21KJB460003.

Data Availability Statement: Data is contained within the article.

Conflicts of Interest: The authors declare no conflict of interest.

References

- Blanes, C.; Ortiz, C.; Mellado, M.; Beltrán, P. Assessment of eggplant firmness with accelerometers on a pneumatic robot gripper. *Comput. Electron. Agric.* **2015**, *113*, 44–50. [[CrossRef](#)]
- Ji, W.; Qian, Z.; Xu, B.; Chen, G.; Zhao, D. Apple viscoelastic complex model for bruise damage analysis in constant velocity grasping by gripper. *Comput. Electron. Agric.* **2019**, *162*, 907–920. [[CrossRef](#)]
- Xiong, Y.; Peng, C.; Grimstad, L.; From, P.J.; Isler, V. Development and field evaluation of a strawberry harvesting robot with a cable-driven gripper. *Comput. Electron. Agric.* **2019**, *157*, 392–402. [[CrossRef](#)]
- Endo, G.; Otomo, N. Development of a food handling gripper considering an appetizing presentation. In Proceedings of the 2016 IEEE International Conference on Robotics and Automation (ICRA), Stockholm, Sweden, 16–21 May 2016; pp. 4901–4906.
- Wang, Z.; Hirai, S. A Soft Gripper with Adjustable Stiffness and Variable Working Length for Handling Food Material. In Proceedings of the 2018 IEEE International Conference on Real-Time Computing and Robotics (RCAR), Kandima, Maldives, 1–5 August 2018; pp. 25–29.
- Kuriyama, Y.; Okino, Y.; Wang, Z.; Hirai, S. A Wrapping Gripper for Packaging Chopped and Granular Food Materials. In Proceedings of the 2019 2nd IEEE International Conference on Soft Robotics (RoboSoft), Seoul, Republic of Korea, 14–18 April 2019; pp. 114–119.
- Wang, Z.; Or, K.; Hirai, S. A dual-mode soft gripper for food packaging. *Robot. Auton. Syst.* **2020**, *125*, 103427. [[CrossRef](#)]
- Kim, U.; Seok, D.-Y.; Kim, Y.B.; Lee, D.-H.; Choi, H.R. Development of a grasping force-feedback user interface for surgical robot system. In Proceedings of the 2016 IEEE/RSJ International Conference on Intelligent Robots and Systems (IROS), Daejeon, Republic of Korea, 9–14 October 2016; pp. 845–850.
- Gerboni, G.; Brancadoro, M.; Tortora, G.; Diodato, A.; Cianchetti, M.; Menciassi, A. A novel linear elastic actuator for minimally invasive surgery: Development of a surgical gripper. *Smart Mater. Struct.* **2016**, *25*, 105025. [[CrossRef](#)]
- Guo, J.; Low, J.-H.; Liang, X.; Lee, J.S.; Wong, Y.-R.; Yeow, R.C.H. A Hybrid Soft Robotic Surgical Gripper System for Delicate Nerve Manipulation in Digital Nerve Repair Surgery. *IEEE/ASME Trans. Mechatron.* **2019**, *24*, 1440–1451. [[CrossRef](#)]
- Sun, Y.; Liu, Y.; Pancheri, F.; Lueth, T.C. Larg: A lightweight robotic gripper with 3-D topology optimized adaptive fingers. *IEEE/ASME Trans. Mechatron.* **2022**, *27*, 2026–2034. [[CrossRef](#)]
- Sun, Y.; Liu, Y.; Xu, L.; Zou, Y.; Faragasso, A.; Lueth, T.C. Automatic design of compliant surgical forceps with adaptive grasping functions. *IEEE Robot. Autom. Lett.* **2020**, *5*, 1095–1102. [[CrossRef](#)]
- Liu, C.-H.; Chiu, C.-H. Optimal design of a soft robotic gripper with high mechanical advantage for grasping irregular objects. In Proceedings of the 2017 IEEE International Conference on Robotics and Automation (ICRA), Singapore, 29 May–3 June 2017; pp. 2846–2851.

14. Liu, C.-H.; Huang, G.-F.; Chiu, C.-H.; Chen, T.-L. Topology and size optimization of an adaptive compliant gripper to maximize the geometric advantage. In Proceedings of the 2016 IEEE International Conference on Advanced Intelligent Mechatronics (AIM), Banff, AB, Canada, 12–15 July 2016; pp. 1145–1150.
15. Hua, H.; Song, J.; Zhao, J.; Liao, Z. Sensor-less Grasping Force Control of a Pneumatic Underactuated Robotic Gripper. *J. Mech. Robot.* **2023**, *16*, 031005. [[CrossRef](#)]
16. Hua, H.; Liao, Z.; Zhao, J. Design, Analysis, and Experiment of an Underactuated Robotic Gripper Actuated by Linear Series Elastic Actuator. *J. Mech. Robot.* **2022**, *15*, 021002. [[CrossRef](#)]
17. Hua, H.; Liao, Z.; Wu, X.; Chen, Y.; Feng, C. A Back-drivable Linear Force Actuator for Adaptive Grasping. *J. Mech. Sci. Technol.* **2022**, *36*, 4213–4220. [[CrossRef](#)]
18. Odhner, L.U.; Jentoft, L.P.; Claffee, M.R.; Corson, N.; Tenzer, Y.; Ma, R.R.; Buehler, M.; Kohout, R.; Howe, R.D.; Dollar, A.M. A compliant, underactuated hand for robust manipulation. *Int. J. Robot. Res.* **2014**, *33*, 736–752. [[CrossRef](#)]
19. Romeo, R.A.; Zocco, A.; Fiorio, L.; Pucci, D.; Maggiali, M. Force control with friction compensation in a pneumatic gripper. In Proceedings of the 2021 IEEE/RISJ International Conference on Intelligent Robots and Systems (IROS), Prague, Czech Republic, 27 September–1 October 2021; pp. 7231–7237.
20. Romeo, R.A.; Fiorio, L.; L’Erario, G.; Maggiali, M.; Metta, G.; Pucci, D. Dynamic control of a rigid pneumatic gripper. *IEEE Robot. Autom. Lett.* **2020**, *5*, 2793–2800. [[CrossRef](#)]
21. Zhang, T.; Jiang, L.; Wu, X.; Feng, W.; Zhou, D.; Liu, H. Fingertip three-axis tactile sensor for multifingered grasping. *IEEE/ASME Trans. Mechatron.* **2014**, *20*, 1875–1885. [[CrossRef](#)]
22. Jentoft, L.P.; Dollar, A.M.; Wagner, C.R.; Howe, R.D. Intrinsic embedded sensors for polymeric mechatronics: Flexure and force sensing. *Sensors* **2014**, *14*, 3861–3870. [[CrossRef](#)]
23. Kim, U.; Lee, D.; Yoon, W.J.; Hannaford, B.; Choi, H.R. Force sensor integrated surgical forceps for minimally invasive robotic surgery. *IEEE Trans. Robot.* **2015**, *31*, 1214–1224. [[CrossRef](#)]
24. Li, Y.; Cao, Y.; Jia, F. A Neural Network Based Dynamic Control Method for Soft Pneumatic Actuator with Symmetrical Chambers. *Actuators* **2021**, *10*, 112. [[CrossRef](#)]
25. Chavoshian, M.; Taghizadeh, M.; Mazare, M. Hybrid dynamic neural network and PID control of pneumatic artificial muscle using the PSO algorithm. *Int. J. Autom. Comput.* **2020**, *17*, 428–438. [[CrossRef](#)]
26. Pratt, J.E.; Krupp, B.T. Series elastic actuators for legged robots: Unmanned Ground Vehicle Technology VI. In Proceedings of the Defense and Security, Orlando, FL, USA, 12–16 April 2004; pp. 135–144.
27. Wensing, P.M.; Wang, A.; Seok, S.; Otten, D.; Lang, J.; Kim, S. Proprioceptive actuator design in the mit cheetah: Impact mitigation and high-bandwidth physical interaction for dynamic legged robots. *IEEE Trans. Robot.* **2017**, *33*, 509–522. [[CrossRef](#)]
28. Tsagarakis, N.G.; Laffranchi, M.; Vanderborght, B.; Caldwell, D.G. A compact soft actuator unit for small scale human friendly robots. In Proceedings of the 2009 IEEE International Conference on Robotics and Automation, Kobe, Japan, 12–17 May 2009; pp. 4356–4362.
29. Shi, Y.; Zhang, M.; Zhang, X.; Bai, F. Design and analysis of a rotary-type robot flexible joint. *China Mech. Eng.* **2016**, *27*, 2494.
30. Kong, K.; Bae, J.; Tomizuka, M. Control of rotary series elastic actuator for ideal force-mode actuation in human–robot interaction applications. *IEEE/ASME Trans. Mechatron.* **2009**, *14*, 105–118. [[CrossRef](#)]
31. Kong, K.; Bae, J.; Tomizuka, M. A Compact Rotary Series Elastic Actuator for Knee Joint Assistive System. In Proceedings of the IEEE International Conference on Robotics & Automation, Anchorage, AK, USA, 3–7 May 2010; pp. 2940–2945.
32. Kong, K.; Bae, J.; Tomizuka, M. A Compact Rotary Series Elastic Actuator for Human Assistive Systems. *IEEE/ASME Trans. Mechatron.* **2012**, *17*, 288–297. [[CrossRef](#)]

Disclaimer/Publisher’s Note: The statements, opinions and data contained in all publications are solely those of the individual author(s) and contributor(s) and not of MDPI and/or the editor(s). MDPI and/or the editor(s) disclaim responsibility for any injury to people or property resulting from any ideas, methods, instructions or products referred to in the content.